Supporting Information

$K_x[Bi_{4-x}Mn_xS_6]$, Design of a Highly Selective Ion Exchange Material and Direct Gap 2D Semiconductor

Ruiqi Wang,[a] Haijie Chen,[b] Yi Xiao,[a] Ido Hadar,[b] Kejun Bu,[c] Xian Zhang,[d] Jie Pan,[c] Yuhao Gu,[a] Zhongnan Guo,[b] Fuqiang Huang,[*,a,c] Mercouri G. Kanatzidis[*,b]

[a] *Beijing National Laboratory for Molecular Sciences and State Key Laboratory of Rare Earth Materials Chemistry and Applications, College of Chemistry and Molecular Engineering, Peking University, Beijing 100871, China*

[b] *Department of Chemistry, Northwestern University, 2145 Sheridan Road, Evanston, Illinois 60208, United States*

[c] *CAS Key Laboratory of Materials for Energy Conversion and State Key Laboratory of High-Performance Ceramics and Superfine Microstructure, Shanghai Institute of Ceramics, Chinese Academy of Sciences, Shanghai 200050, P. R. China*

[d] *Qian Xuesen Laboratory of Space Technology, China Academy of Space Technology, Beijing 100094, P. R. China*

List of contents:

1. **Experimental section**
2. **Results and discussion**
3. **Supplementary figures**
4. **Supplementary tables**

1. Experimental section.

Powder X-ray Diffraction. Powder X-ray diffraction (PXRD) measurements were performed on ground crystalline samples using a Bruker D2 Phaser diffractometer equipped with a monochromatized source of Cu $K\alpha$ radiation (λ = 0.15406 nm) at 4 kW (40 kV, 100 mA). The patterns were collected with 2θ from 5° to 80° with a scan-rate of 1.2° min^{-1}.

Scanning Electron Microscopy. A Phenom Pro scanning electron microscope (SEM) equipped with a Princeton Gamma Tech (PGT) energy-dispersive X-ray analyzer was used to acquire images and semi-quantitative energy dispersive X-ray spectroscopy (EDS). Single crystals were picked and placed on the surface of a double-sided carbon-aluminum tape which was attached on the aluminum SEM substrate. EDS spectra were collected by using an accelerating voltage of 15 keV with a 60 s accumulation time.

Solid State Ultraviolet-Visible Spectroscopy. The ultraviolet-visible (UV-vis) light diffuse-reflectance spectrum was measured on a UV-4100 spectrophotometer operating from 2500 nm to 300nm. The fine powder was spread on a compacted base of compressed $BaSO_4$ (100 % reflectance standard). The reflectance-versus-wavelength data were used to obtain the band gap. The reflectance data were converted to absorbance using the Kubelka-Munk equation.

Thermal Analysis. Differential scanning calorimetry (DSC) analysis was performed using a Thermal Analysis SDT2960 thermal analyzer under N_2 flow. Well-ground powder was loaded into a silica crucible placed on the sample side of the detector, with an empty crucible on the reference side. The temperature rate of heating and cooling were ±15 °C/min, and the maximum temperature was 850 °C. The DSC product was examined by PXRD.

X-ray Photoelectron Spectroscopy (XPS). The oxidation states Mn in $K_x[Bi_{4-x}Mn_xS_6]$ (x = 1.28) and the Cs^+-exchanged product were determined by XPS using an Axis Ultra spectrometer. The binding energies were corrected against the reference C 1*s* (284.5 eV).

2. Results and discussion

Isotherm and Kinetic Studies of Cs^+ Ion Exchange. Because of the change in the Mn^{2+} oxidation during the Cs^+ exchange process in air, isotherm and kinetic studies were carried out in both air and in Ar atmosphere. As depicted in **Figure S12a**, the Cs^+ sorption capacities in Ar were obviously higher than those in air. The difference in capacities results from the Mn^{2+} oxidation by O_2 in air which reduces the demand of Cs^+ to balance charge. The sorption capacity in air is atypical as it increases linearly along with the increasing equilibrium concentration. The difference between adsorption capacities in Ar and air tends to be smaller along with the increasing Cs^+ concentration in the solution, indicating that the Mn^{2+} oxidation can be restrained by higher Cs^+ concentration. The linear adsorption curve in air should be caused by the concomitant change in the oxidation of Mn^{2+} by the changing Cs^+ concentration in the solution. In Ar gas the sorption isotherm curve can be fitted with a high correlation coefficient $R^2 \sim 0.974$ by the Freundlich model (1),

$$q = K_F C_e^{1/n} \quad (1)$$

where K_F is the Freundlich constant. This model does not provide the maximum capacity. It was obtained by averaging Cs^+ uptake values in the plateau of the isotherm curve, which represents the saturation adsorption. The maximum capacity 164 mg/g is lower than the theoretical capacity of 193 mg/g, which might be caused by the O_2 dissolved in water causing some Mn^{2+} oxidation.

The oxidation of Mn^{2+} to Mn^{3+} is topotactic (i.e the structure of the material remains the same) and it is an O_2-dependent process that also affects the adsorption of Cs^+ by $K_x[Bi_{4-x}Mn_xS_6]$ (x = 1.28) because the overall change of the layers is decreased. A complex adsorption and release behavior was observed when we conducted the kinetic study in air. The Cs^+ concentration decreased steeply and reached the minimum within 15 min. After that, the Cs^+ concentration in solution increased and reached the equilibrium within 300 min. There exist two competitive processes during the Cs^+ exchange in $K_x[Bi_{4-x}Mn_xS_6]$ and KMS-1($K_{2x}Mn_xSn_{3-x}S_6$), one is the replacement of K^+ by Cs^+, the other is the fast oxidation of Mn^{2+} by the environmental oxygen which leads to the release of the intercalated Cs^+. If the fast dynamics of the latter process is suppressed, the intercalated Cs^+ will release slowly. This phenomenon was observed in the Cs^+-exchanging process of $K_x[Bi_{4-x}Mn_xS_6]$ rather than KMS-1, which indicates that the dynamics of Mn^{2+} oxidation in $K_x[Bi_{4-x}Mn_xS_6]$ is slower than that in KMS-1. It also suggests that the binding of the $[Bi_{2.72}Mn_{1.28}S_6]^{1.28-}$ layers to Cs^+ is weaker than the KMS-1 layers $[MnSn_2S_6]^-$. For both compounds Mn^{2+} is oxidized by atmospheric oxygen. In KMS-1, each Mn^{2+} ion in the single-octahedral-layered $[MnSn_2S_6]^-$ slabs can simultaneously contact with oxygen from both sides of the slab, while in thicker-layered $[Mn_xBi_{4-x}S_6]^{x-}$ imposes a longer distance (on average) between the Mn^{2+} and O_2 atoms slowing down the electron transfer kinetics. The specific Cs^+ adsorption dynamics of $K_x[Bi_{4-x}Mn_xS_6]$ (x = 1.28) can quickly extract Cs^+ ion from low concentration solutions and release these ions in other solutions implying the possibility to recycle and reuse the material. The kinetic study of Cs^+ exchange in Ar revealed that the Cs^+ concentration decreased steeply from 100 ppm to 36 ppm within 40 min, as shown in **Figure S12b**. The final Cs^+ concentration after 24 h adsorption was 25 ppm, which is much lower than that of kinetic in air.

3. Supplementary figures.

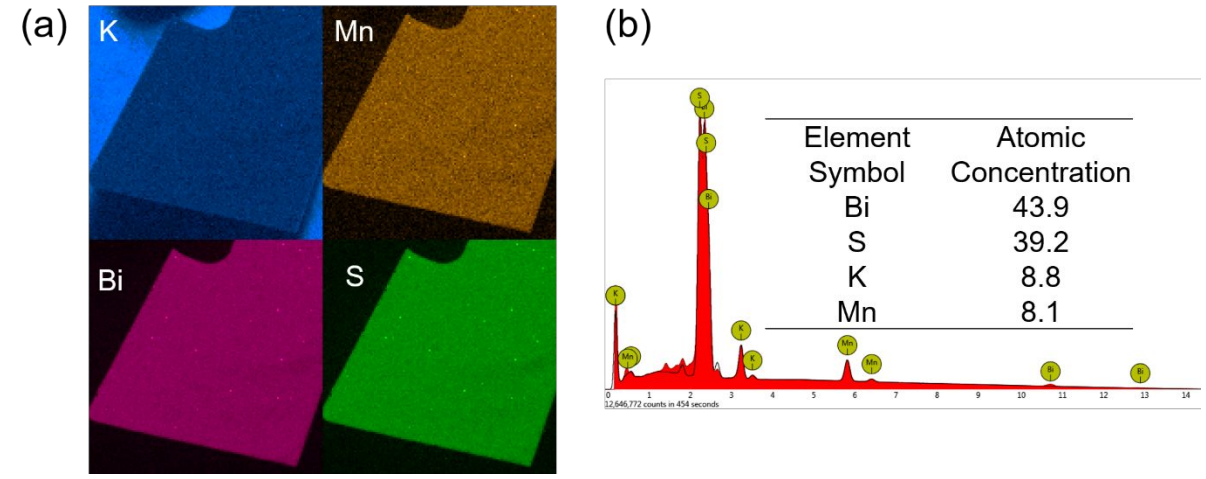

Figure S1. (a) EDS mapping images of K, Mn, Bi and S. (b) EDS spectrum and element contents of $K_x[Bi_{4-x}Mn_xS_6]$ (x = 1.28).

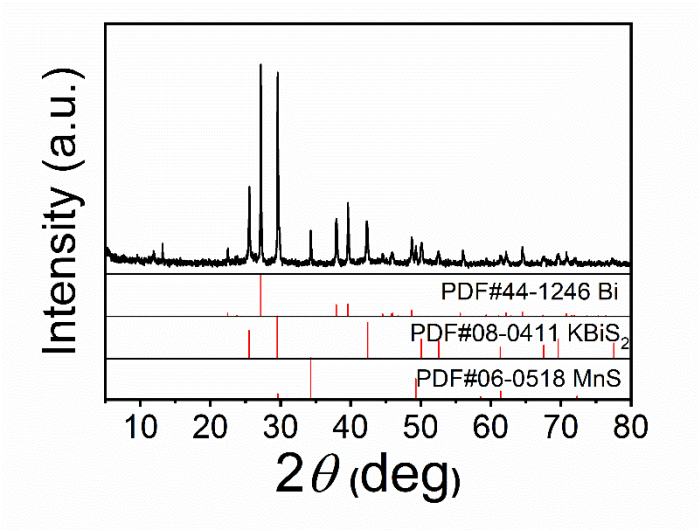

Figure S2. PXRD pattern of the product obtained after DSC analysis.

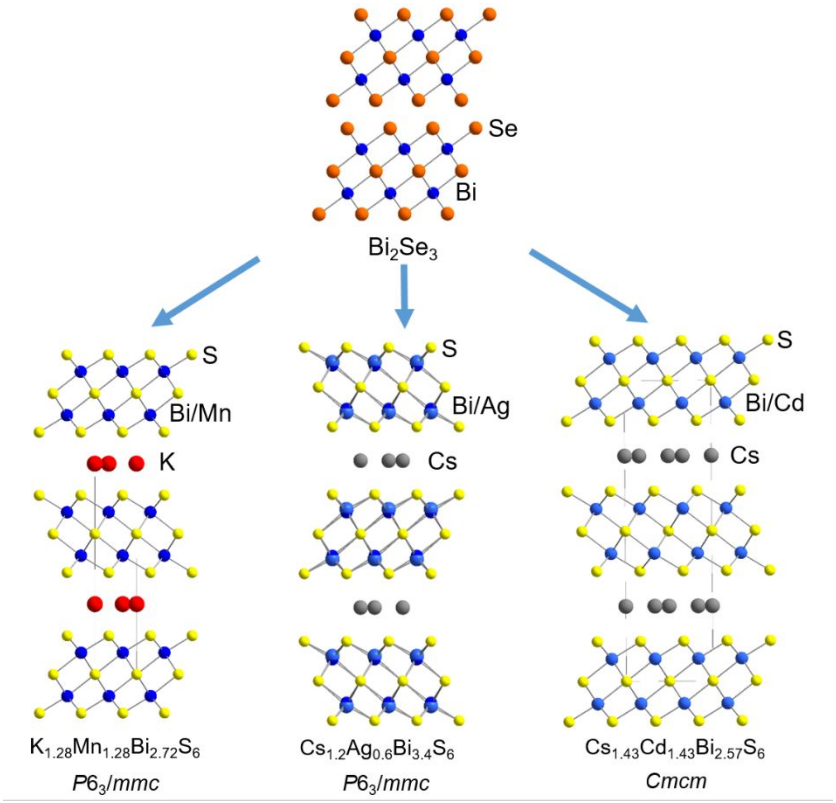

Figure S3. Structure comparison between Bi_2Se_3, $K_{1.28}Mn_{1.28}Bi_{2.72}S_6$, $Cs_{1.2}Ag_{0.6}Bi_{3.4}S_6$ and $Cs_{1.43}Cd_{1.43}Bi_{2.57}S_6$.

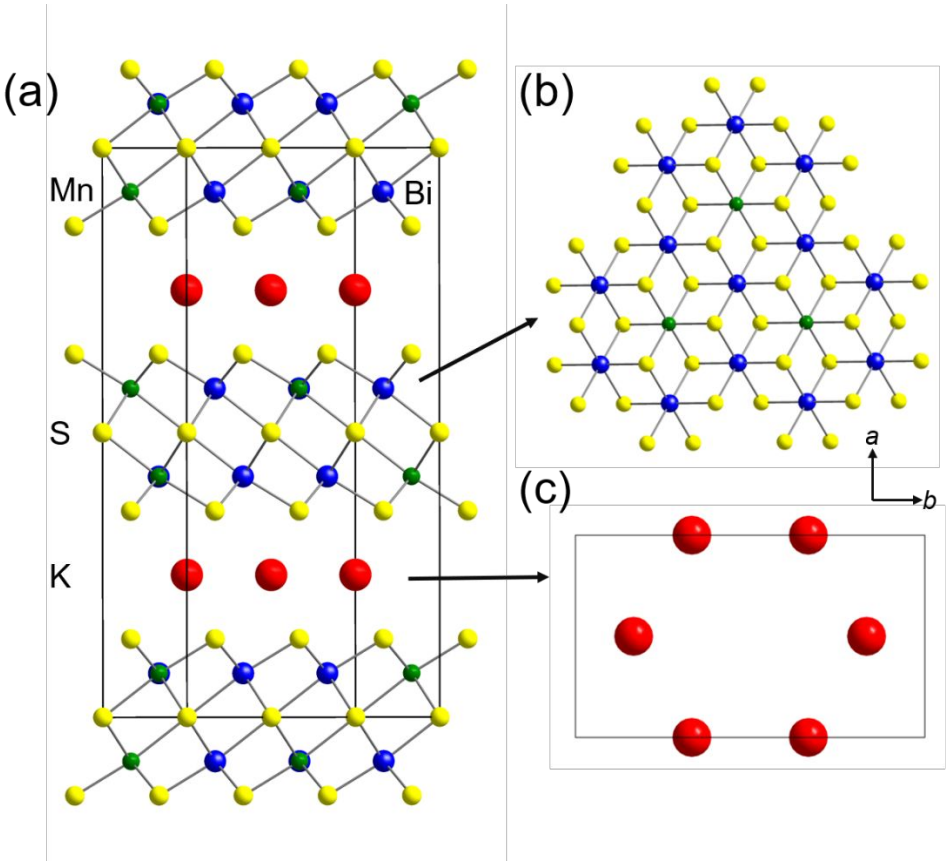

Figure S4. (a) Schematic diagram of the unit cell of $K_2Bi_4Mn_2S_9$ (*Cmcm*) with ordered Mn and Bi arrangement. This model was used to perform the DFT calculations. (b) sublayer of $[Bi_4Mn_2S_9]^{2-}$ and (c) K^+ layer viewed down [001].

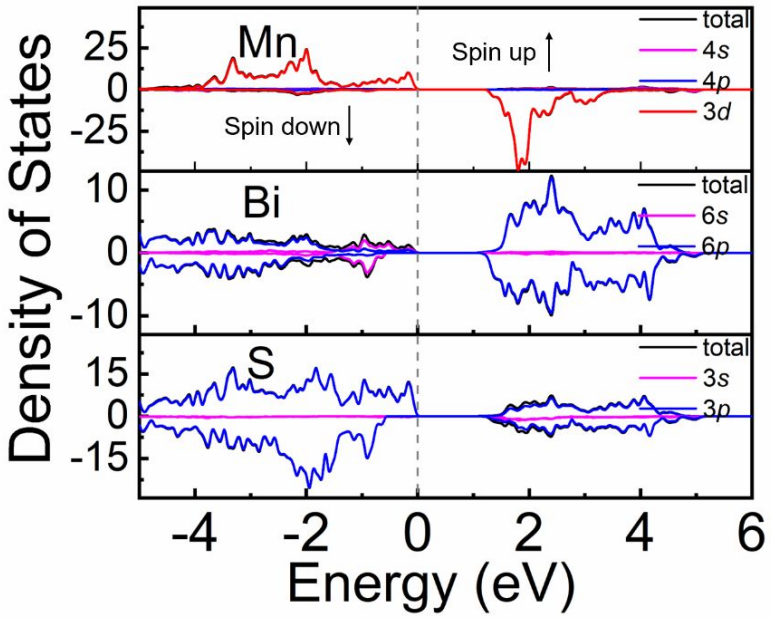

Figure S5. Orbital-resolved spin-polarized Partial DOS of Mn, Bi and S of $K_2Bi_4Mn_2S_9$. The negative energies are filled states. The spin-up Mn 3*d* states are fully occupied while the spin-down states are empty, which indicate high-spin state (HS) Mn^{2+} ions.

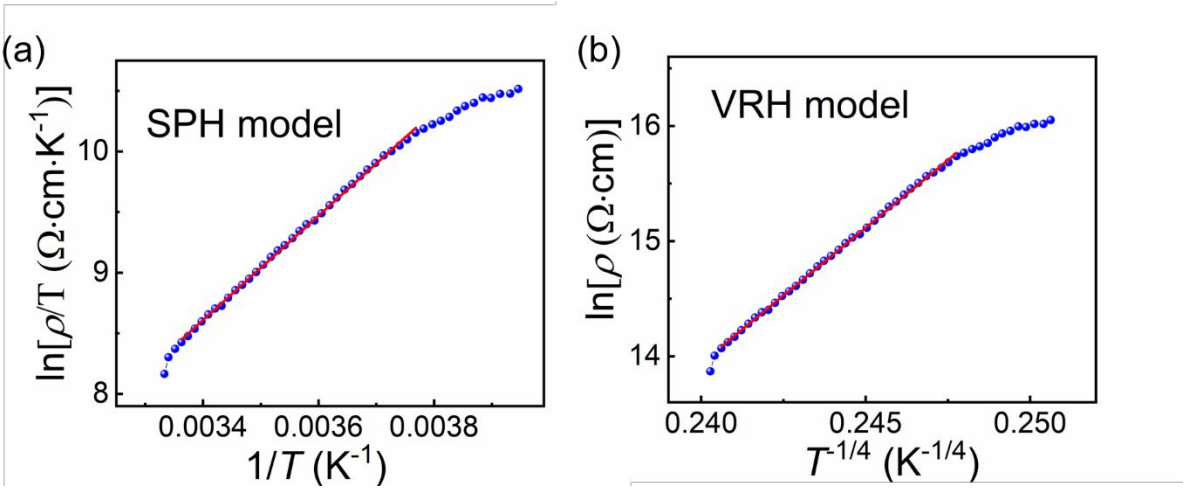

Figure S6. (a) $ln(\rho/T)$ vs T^{-1} plot of the SPH model (E_p = 0.37 eV) and (b) $ln(\rho)$ vs $T^{-1/4}$ plot of the VRH model (T_0 = 235 K).

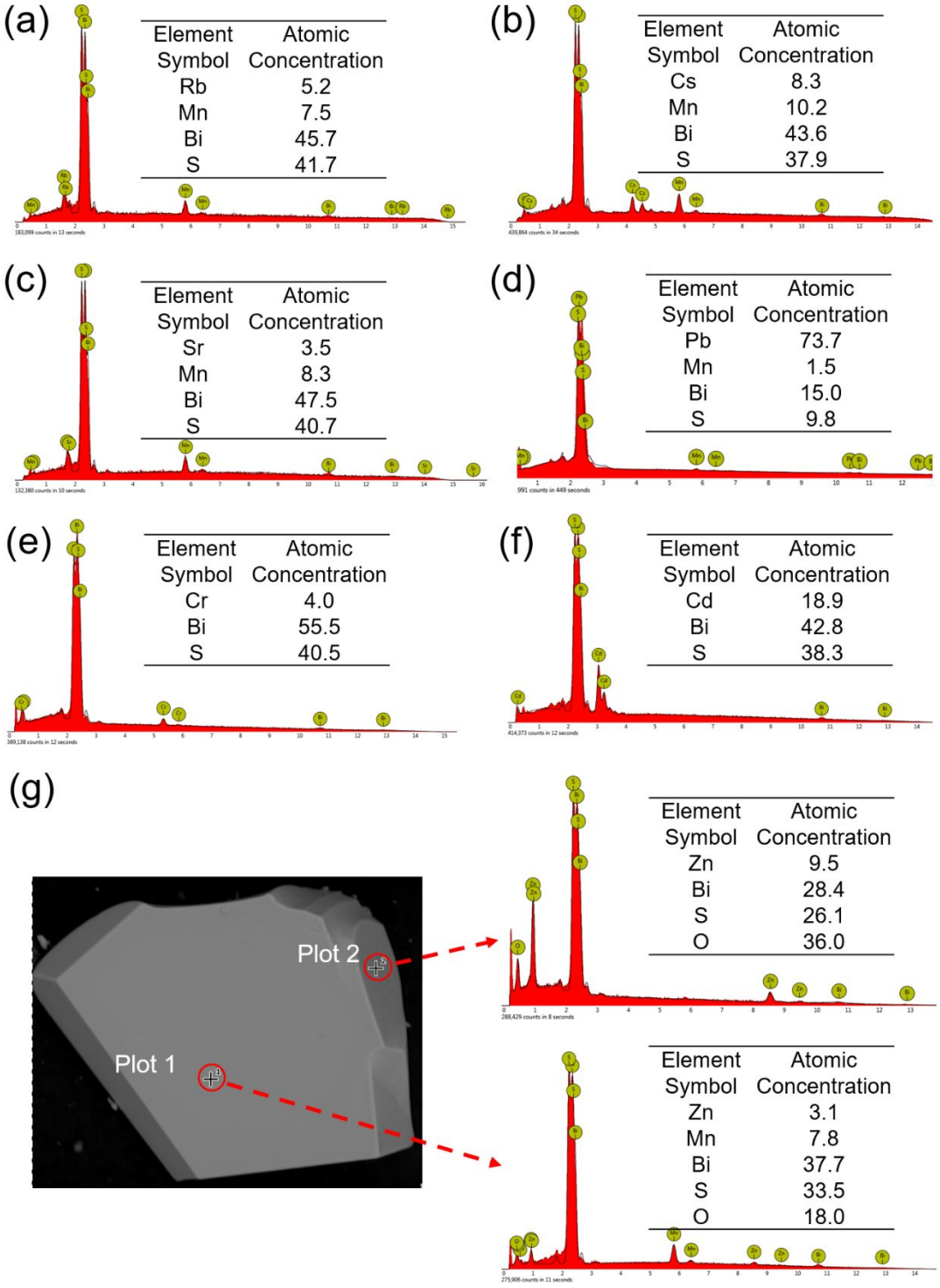

Figure S7. EDS spectra and semi-quantitative contents of (a) Rb^{+}, (b) Cs^{+}, (c) Sr^{2+}, (d) Pb^{2+}, (e) Cr^{3+}, (f) Cd^{2+} and (g) Zn^{2+}-exchanged products of $K_x[Bi_{4-x}Mn_xS_6]$ (x = 1.28). The contents of Bi and S obtained by EDS spectra are inaccurate because of the overlap of the characteristic peaks of Bi ($M\alpha$ 2.41 keV) and S ($K\alpha$1 2.31 keV).

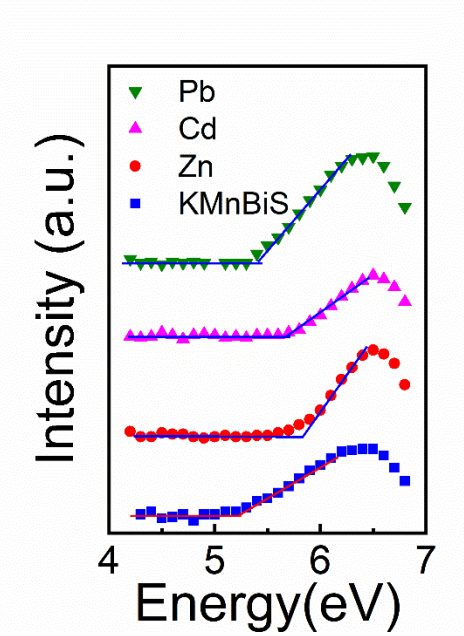

Figure S8. Photoelectron spectroscopy in air (PESA) of $K_x[Bi_{4-x}Mn_xS_6]$ (x = 1.28) and Zn^{2+}, Cd^{2+} and Pb^{2+} exchanged products.

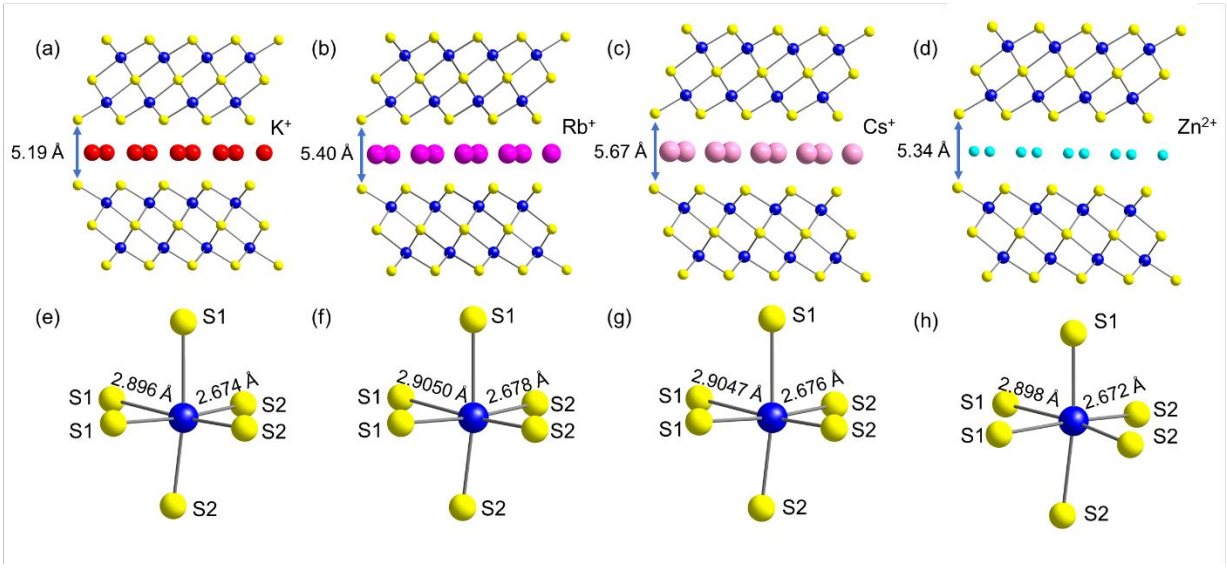

Figure S9. The crystal structures of (a) $K_x[Bi_{4-x}Mn_xS_6]$, (b) Rb^+-, (c) Cs^+-, and (d) Zn^{2+}-exchanged products. The Mn/BiS_6 octahedra in the structures of (e) $K_x[Bi_{4-x}Mn_xS_6]$, (f) Rb^+-, (g) Cs^+-, and (h) Zn^{2+}-exchanged products with the indications of Mn/Bi–S bond lengths.

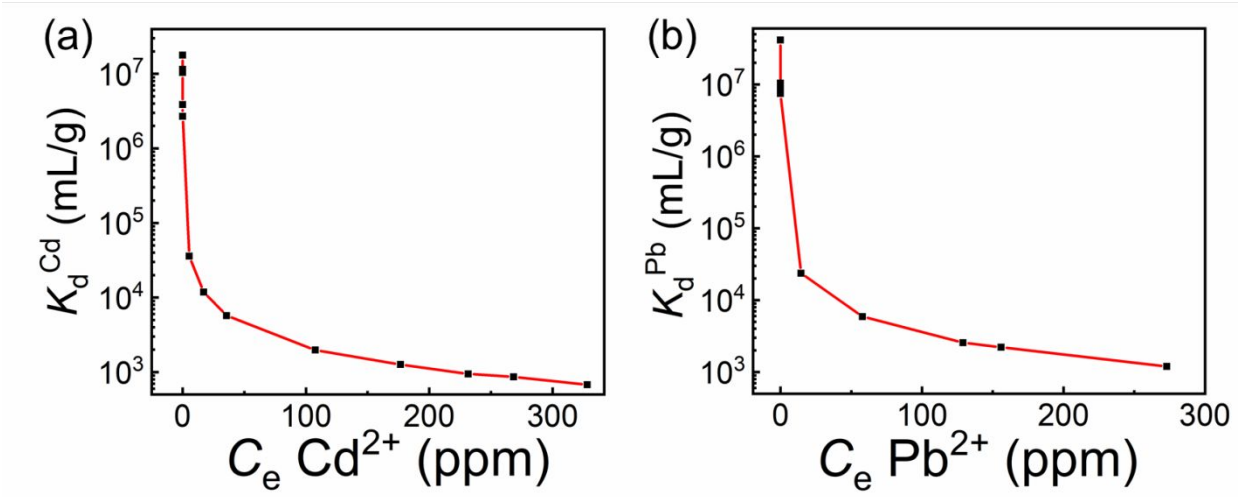

Figure S10. Distribution coefficient K_d of (a) Cd^{2+} and (b) Pb^{2+} ion exchange.

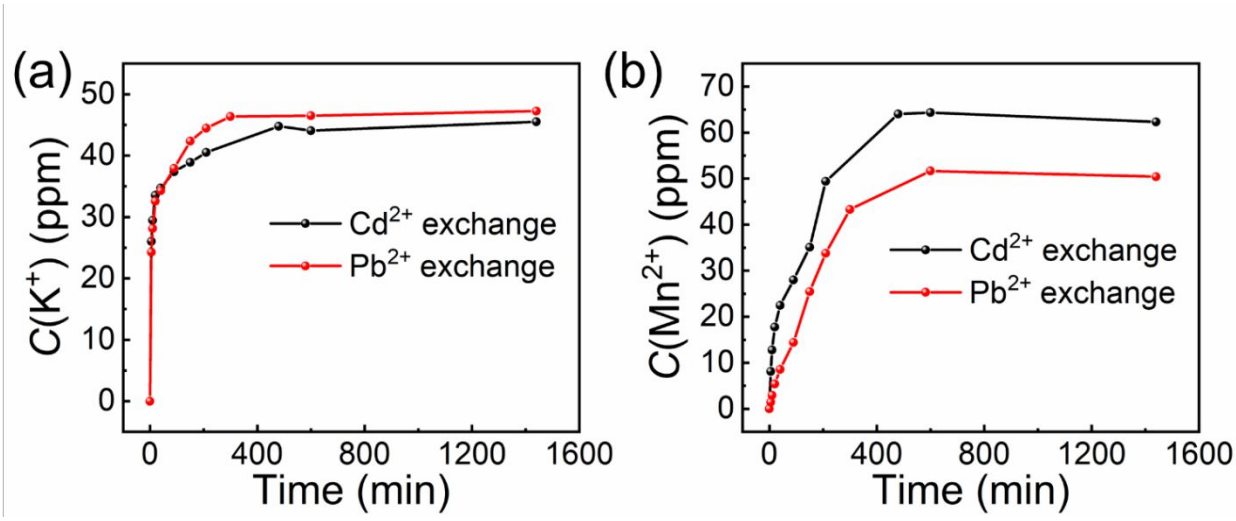

Figure S11. The release kinetics of (a) K^+ and (b) Mn^{2+} for Cd^{2+} and Pb^{2+} ion exchange.

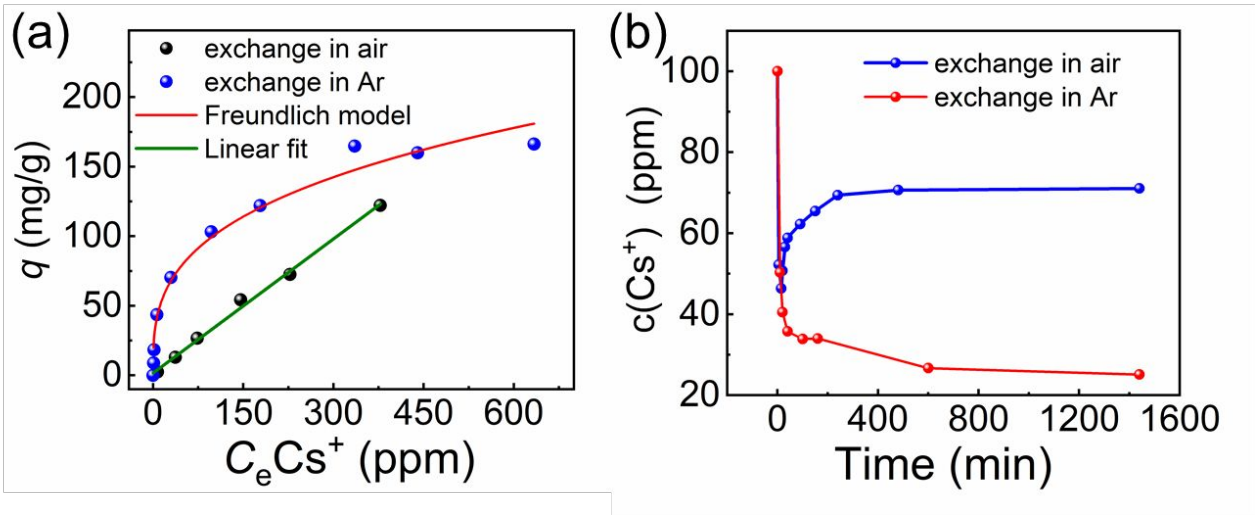

Figure S12. (a) Sorption isotherm curve for Cs^+ ion exchange in air and Ar atmosphere. The blue and black point plots represent the data of ion exchange in Ar and air, respectively. The red solid line represents the fitting of the data with the Freundlich model (fitting data: K_F = 23(4) L/g, n = 3.1(0.3)). The green solid line represents the linear fitting of data. (b) Kinetic of Cs^+ ion exchange in air and Ar with the initial Cs^+ concentration of 100 ppm.

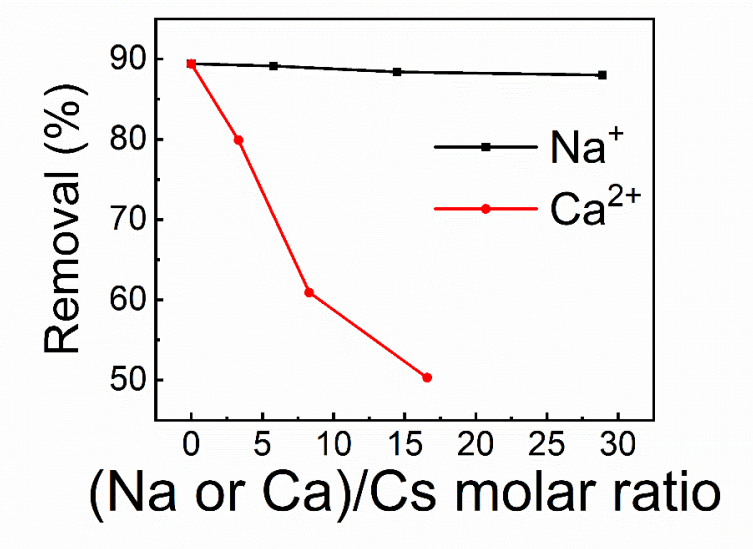

Figure S13. Removal of Cs^+ in various concentration solution of NaCl or $CaCl_2$ in Ar, the initial concentration of Cs^+ is 10 ppm

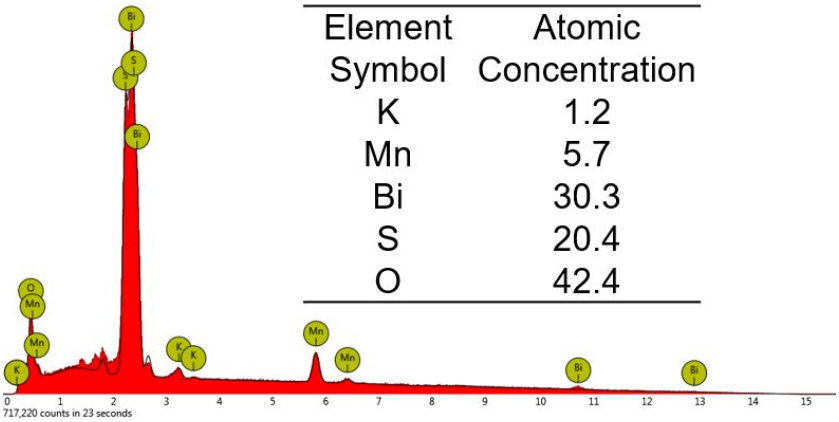

Element Symbol	Atomic Concentration
K	1.2
Mn	5.7
Bi	30.3
S	20.4
O	42.4

1

2 **Figure S14**. EDS spectrum and element contents of the product treated in pH = 11.5 solution.

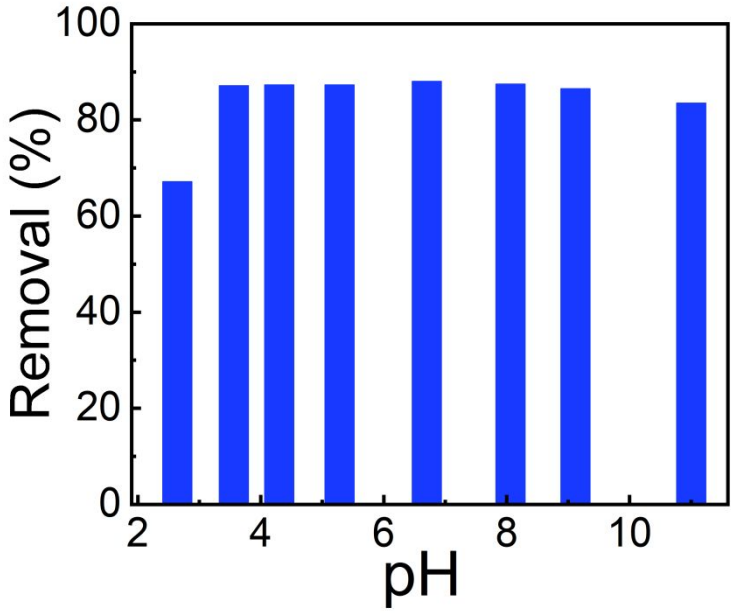

3

4 **Figure S15** Removal of Cs^+ in solutions of various pH (2.6–11) in Ar, the initial

5 concentration of Cs^+ is 10 ppm

4. **Supplementary tables.**

Table S1. Atomic coordinates and equivalent isotropic displacement parameters (Å^2) of $K_{1.28}Mn_{1.28}Bi_{2.72}S_6$ at 180 K

Label	x	y	z	Occupancy	U_{eq}*
Mn1	0.6667	0.3333	0.57724(2)	0.320(1)	0.0148(2)
Bi1	0.6667	0.3333	0.57724(2)	0.680(1)	0.0148(2)
S1	1.0000	0	0.5000	1	0.0211(8)
S2	0.3333	0.6667	0.6376(2)	1	0.0230(6)
K1	0.6667	0.3333	0.7500	0.21(2)	0.039(5)
K2	0	1.0000	0.7500	0.43(2)	0.13(1)

*U_{eq} is defined as one third of the trace of the orthogonalized U_{ij} tensor.

Table S2. Anisotropic displacement parameters (Å^2) of $K_{1.28}Mn_{1.28}Bi_{2.72}S_6$ at 180 K

Label	U_{11}	U_{22}	U_{33}	U_{12}	U_{13}	U_{23}
Mn1	0.0143(2)	0.0143(2)	0.0155(3)	0.0072(1)	0	0
Bi1	0.0143(2)	0.0143(2)	0.0155(3)	0.0072(1)	0	0
S1	0.0227(11)	0.0227(11)	0.0181(16)	0.0113(6)	0	0
S2	0.0201(8)	0.0201(8)	0.0288(13)	0.0100 (4)	0	0
K1	0.052(7)	0.052(7)	0.014(7)	0.026(3)	0	0
K2	0.187(17)	0.187(17)	0.013(5)	0.094(9)	0	0

Table S3. Selected bond lengths and angles for $Rb_{0.88}Mn_{1.28}Bi_{2.72}S_6$

bond type	distance (Å)	angle type	angle (°)
Bi–S1×3	2.9050(9)	S1–Bi–S1×3	85.74(3)
Bi–S2×3	2.678(4)	S2–Bi–S2×3	95.1(2)
Rb1–S2×6	3.535(6)	S2–Bi–S1×2	89.4(2)
Rb2–S2×6	3.535(6)	S2–Bi–S1×2	89.4(2)

Table S4. Selected bond lengths and angles for $Cs_{1.03}Mn_{1.28}Bi_{2.72}S_6$

bond type	distance (Å)	angle type	angle (°)
Bi–S1×3	2.9047(4)	S1–Bi–S1×3	85.81(2)
Bi–S2×3	2.676(2)	S2–Bi–S2×3	95.3(2)
Cs1–S2×6	3.640(4)	S2–Bi–S1×2	89.24(6)
Cs2–S2×6	3.640(4)	S2–Bi–S1×2	89.24(6)

Table S5. Atomic coordinates and equivalent isotropic displacement parameters (Å^2) of $Rb_{0.88}Mn_{1.28}Bi_{2.72}S_6$ at 180 K

Label	x	y	z	Occupancy	U_{eq}*
Mn1	0.6667	0.3333	0.42383(4)	0.320(2)	0.0198(5)
Bi1	0.6667	0.3333	0.42383(6)	0.680(2)	0.0198(5)
S1	1.0000	0	0.5000	1	0.029(3)
S2	0.3333	0.6667	0.3644(3)	1	0.029(2)
Rb1	0.6667	0.3333	0.2500	0.17(3)	0.07(2)
Rb2	1.0000	0	0.2500	0.27(3)	0.12(2)

*U_{eq} is defined as one third of the trace of the orthogonalized U_{ij} tensor.

Table S6. Anisotropic displacement parameters (Å^2) of $Rb_{0.88}Mn_{1.28}Bi_{2.72}S_6$ at 180 K

Label	U_{11}	U_{22}	U_{33}	U_{12}	U_{13}	U_{23}
Mn1	0.0153(6)	0.0153(6)	0.0288(8)	0.0077(3)	0	0
Bi1	0.0153(6)	0.0153(6)	0.0288(8)	0.0077(3)	0	0
S1	0.023(4)	0.023(4)	0.040(6)	0.011(2)	0	0
S2	0.024(2)	0.024(2)	0.041(4)	0.012(2)	0	0
Rb1	0.10(3)	0.10(3)	0.02(2)	0.05(2)	0	0
Rb2	0.17(3)	0.17(3)	0.04(2)	0.08(2)	0	0

Table S7. Atomic coordinates and equivalent isotropic displacement parameters (Å^2) of $Cs_{1.03}Mn_{1.28}Bi_{2.72}S_6$ at 180 K

Label	x	y	z	Occupancy	U_{eq}*
Mn1	0.6667	0.3333	0.42550(3)	0.320(2)	0.0158(3)
Bi1	0.6667	0.3333	0.42550(3)	0.680(2)	0.0158(3)
S1	1.0000	0	0.5000	1	0.025(2)
S2	0.3333	0.6667	0.3676(2)	1	0.0231(9)
Cs1	0.6667	0.3333	0.2500	0.20(2)	0.056(6)
Cs2	0	1.0000	0.2500	0.32(2)	0.089(5)

*U_{eq} is defined as one third of the trace of the orthogonalized U_{ij} tensor.

Table S8. Anisotropic displacement parameters (Å^2) of $Cs_{1.03}Mn_{1.28}Bi_{2.72}S_6$ at 180 K

Label	U_{11}	U_{22}	U_{33}	U_{12}	U_{13}	U_{23}
Mn1	0.0155(4)	0.0155(4)	0.0164(4)	0.0078(2)	0	0
Bi1	0.0155(4)	0.0155(4)	0.0164(4)	0.0078(2)	0	0
S1	0.0231(2)	0.0231(2)	0.028(3)	0.0116(8)	0	0
S2	0.022(2)	0.022(2)	0.025(2)	0.0038(4)	0	0
Cs1	0.076(8)	0.076(8)	0.021(5)	0.038(4)	0	0
Cs2	0.123(8)	0.123(8)	0.021(3)	0.061(4)	0	0

Table S9. Crystallographic data (180 K) and details of the structure refinement of Zn^{2+}-exchanged single crystal.

Formula	$Zn_{0.64}Mn_{1.28}Bi_{2.72}S_6$
Space group	$P6_3/mmc$
F_w(g·mol^{-1})	872.95
a (Å)	3.9470(2)
c (Å)	23.427(2)
V(Å^3)	316.07(4)
crystal color	black
ρ_c (g·cm^{-3})	4.586
μ (mm^{-1})	41.112
F(000)	373
Data/parameter	145/16
R_{int}	0.0392
$R1[I>2\sigma(I)]$	0.0326
wR_2 (all data)	0.0772
GOF	1.392

Table S10. Selected bond lengths and angles for $Zn_{0.64}Mn_{1.28}Bi_{2.72}S_6$

bond type	distance (Å)	angle type	angle (°)
Bi–S1×3	2.8980(7)	S1–Bi–S1×3	85.84(2)
Bi–S2×3	2.672(3)	S2–Bi–S2×3	95.2(2)
		S2–Bi–S1×4	89.27(9)

Table S11. Atomic coordinates and equivalent isotropic displacement parameters (Å^2) of Zn^{2+}-exchanged single crystal. at 180 K

Label	x	y	z	Occupancy	U_{eq}*
Mn1	0.6667	0.3333	0.57642(5)	0.320(2)	0.0168(5)
Bi1	0.6667	0.3333	0.57642(5)	0.680(2)	0.0168(5)
S1	0	1.0000	0.5000	1	0.025(2)
S2	0.6667	0.3333	0.6360(3)	1	0.025(2)
Zn1	0.3333	0.6667	0.7500	0.13(2)	0.12(4)
Zn2	1.0000	0.0000	0.7500	0.19(2)	0.24(5)

*U_{eq} is defined as one third of the trace of the orthogonalized U_{ij} tensor.

Table S12. Anisotropic displacement parameters (Å^2) of Zn^{2+}-exchanged single crystal at 180 K

Label	U_{11}	U_{22}	U_{33}	U_{12}	U_{13}	U_{23}
Mn1	0.0147(5)	0.0147(5)	0.0211(7)	0.0073(3)	0	0
Bi1	0.0147(5)	0.0147(5)	0.0211(7)	0.0073(3)	0	0
S1	0.022(3)	0.022(3)	0.031(4)	0.011(2)	0	0
S2	0.020(2)	0.020(2)	0.032(3)	0.010(2)	0	0
Zn1	0.17(6)	0.17(6)	0.02(2)	0.09(3)	0	0
Zn2	0.30(7)	0.30(7)	0.13(6)	0.15(3)	0	0

Table S13 Comparison of adsorption capacities q_m and distribution coefficients K_d of various adsorbents for Cd^{2+} and Pb^{2+}.

Target ions	adsorbents	q_m (mg/g)	K_d (mL/g)	Reference
Cd^{2+}	$K_x[Bi_{4-x}Mn_xS_6]$	221.2	2.69×10^6-1.77×10^7	This work
	KMS-1	329	1.16-1.37×10^7	1
	KTS-3	209	6.2×10^2-7.6×10^4	2
	EDTA-LDH	42	n/a	3
	Graphene oxide	106.3	n/a	4
	GO-Zr-P	232.36	n/a	5
	Mg-Al-CO_3-LDH	70.2	n/a	6
	Titanate nanotubes	238.61	n/a	7
Pb^{2+}	$K_x[Bi_{4-x}Mn_xS_6]$	342.4	1.04-4.12×10^7	This work
	KMS-1	319	1.3×10^5-1.4×10^6	1
	KTS-3	280	5.5×10^2-2.1×10^6	2
	K-MPS-1	393.5	5.36×10^5	8
	MoS_4-LDH	290	3.29×10^6	9
	Fe-MoS_4-LDH	346	3.6×10^4-2.6×10^5	10
	MoS_4-Ppy	78	6.1×10^5-1.1×10^7	11
	Mn-MoS_4-LDH	357	2.0×10^6	12
	NC-FeMg LDH	345	n/a	13
	EDTA-LDH	158	n/a	3
	GO-Zr-P	363.42	n/a	5

Reference

1. Manos, M. J.; Kanatzidis, M. G., Sequestration of heavy metals from water with layered metal sulfides. *Chem–Eur. J.* **2009,** *15*, 4779-4784.
2. Sarma, D.; Islam, S. M.; Subrahmanyam, K.; Kanatzidis, M. G., Efficient and selective heavy metal sequestration from water by using layered sulfide $K_{2x}Sn_{4-x}S_{8-x}$ (x = 0.65–1; KTS-3). *J. Mater. Chem. A* **2016,** *4*, 16597-16605.
3. Pérez, M.; Pavlovic, I.; Barriga, C.; Cornejo, J.; Hermosín, M.; Ulibarri, M., Uptake of Cu^{2+}, Cd^{2+} and Pb^{2+} on Zn–Al layered double hydroxide intercalated with edta. *Appl. Clay Sci.* **2006,** *32*, 245-251.
4. Zhao, G.; Li, J.; Ren, X.; Chen, C.; Wang, X., Few-layered graphene oxide nanosheets as superior sorbents for heavy metal ion pollution management. *Environ. Sci. Technol.* **2011,** *45*, 10454-10462.
5. Pourbeyram, S., Effective Removal of Heavy Metals from Aqueous solutions by graphene oxide–zirconium phosphate (GO-Zr-P) nanocomposite. *Ind. Eng. Chem. Res.* **2016,** *55*, 5608-5617.
6. Shan, R.; Yan, L.; Yang, K.; Hao, Y.; Du, B., Adsorption of Cd (II) by Mg-Al-CO_3-and magnetic Fe_3O_4/Mg-Al-CO_3-layered double hydroxides: kinetic, isothermal, thermodynamic and mechanistic studies. *J. Hazard. Mater.* **2015,** *299*, 42-49.
7. Xiong, L.; Chen, C.; Chen, Q.; Ni, J., Adsorption of Pb (II) and Cd (II) from aqueous solutions using titanate nanotubes prepared *via* hydrothermal method. *J. Hazard. Mater.* **2011,** *189*, 741-748.
8. Rathore, E.; Pal, P.; Biswas, K., Layered Metal Chalcophosphate (K-MPS-1) for Efficient, Selective, and ppb Level Sequestration of Pb from Water. *J. Phys. Chem. C* **2017,** *121*, 7959-7966.
9. Ma, L.; Wang, Q.; Islam, S. M.; Liu, Y.; Ma, S.; Kanatzidis, M. G., Highly Selective and Efficient Removal of Heavy Metals by Layered Double Hydroxide Intercalated with the MoS_4^{2-} Ion. *J. Am. Chem. Soc.* **2016,** *138*, 2858-2866.
10. Jawad, A.; Liao, Z.; Zhou, Z.; Khan, A.; Wang, T.; Ifthikar, J.; Shahzad, A.; Chen, Z.; Chen, Z., Fe-MoS_4: An Effective and Stable LDH-Based Adsorbent for Selective Removal of Heavy Metals. *ACS Appl. Mater. Inter.* **2017,** *9*, 28451-28463.
11. Xie, L.; Yu, Z.; Islam, S. M.; Shi, K.; Cheng, Y.; Yuan, M.; Zhao, J.; Sun, G.; Li, H.; Ma, S., Remarkable Acid Stability of Polypyrrole-MoS_4: A Highly Selective and Efficient Scavenger of Heavy Metals Over a Wide pH Range. *Adv. Funct. Mater.* **2018,** *28*. 1800502.
12. Ali, J.; Wang, H.; Ifthikar, J.; Khan, A.; Wang, T.; Zhan, K.; Shahzad, A.; Chen, Z.; Chen, Z., Efficient, stable and selective adsorption of heavy metals by thio-functionalized layered double hydroxide in diverse types of water. *Chem. Eng. J.* **2018,** *332*, 387-397.
13. Ling, L.; Liu, W. J.; Zhang, S.; Jiang, H., Achieving high-efficiency and ultrafast removal of Pb (II) by one-pot incorporation of a N-doped carbon hydrogel into FeMg layered double hydroxides. *J. Mater. Chem. A* **2016,** *4*, 10336-10344.